Springer

KSME

Journal of Mechanical Science and Technology 24 (5) (2010) 1067~1076
www.springerlink.com/content/1738-494x
DOI 10.1007/s12206-010-0322-7

Comparison of thermal fatigue behaviour of ASTM A 213 grade T-92 base and weld tubes †

G. R. Jinu[1], P. Sathiya[1,*], G. Ravichandran[2] and A. Rathinam[2]

[1]*Department of Production Engineering National Institute of Technology, Tiruchirappalli-620 015, TamilNadu, India*
[2]*Welding Research Institute, Bharat Heavy Electricals Limited Tiruchirappalli-620 014, Tamil Nadu, India*

(Manuscript Received June 26, 2009; Revised December 24, 2009; Accepted February 16, 2010)

Abstract

Super-heater tubes are subjected to alternate heating and cooling in power plants causing them to crack and eventually fail. This phenomenon is referred to as "thermal fatigue." In this paper, a laboratory simulation for reproducing the thermal fatigue phenomenon is developed to determine the number of cycles necessary before failure occurs in super-heater tubes. The temperature and strain distributions along the specimen were computed theoretically using ANSYS software for the applied temperature condition. The thermal fatigue test was conducted for both base and shielded metal arc (SMA) welded tubes separately and both passed in the non-destructive tests. These tubes were subjected to thermal cycles from 800ºC (accelerated temperature) to room temperature. Oxy-acetylene heating setup was utilized as a heating source, and a water bath was utilized for quenching purposes. The tests were carried out until open cracks were identified. Surface cracks were identified in the base and weld tubes after 90 and 60 cycles respectively. This study reveals that heating and cooling cause thermal fatigue, initiate cracks in the tubes.

Keywords: Thermal fatigue; T-92 tube; Transverse and Circumferential cracks; Failure analysis

1. Introduction

T-92 tubes are widely used in combined–cycle steam systems due to their greater increased temperature strength and creep behavior as compared to other ferritic alloy steel tubes. T-92 tubes show resistance to thermal fatigue superior to austenitic stainless steels. Thermal fatigue occurs in components subjected to alternating heating and cooling. Under thermal fatigue, crack can initiate, propagate, and eventually cause failure. The reason for the cracking is due to the temperature change in the material that induces thermal expansion (or contraction). If surrounding material or external constraints hinder this expansion, thermal stress occurs. These cyclic thermal stresses cause fatigue similar to that of mechanical stresses. This type of failure usually occurs in power industries where turbulent mixing of fluids causes quick thermal transients in boiler heat exchanger tubes [1].

These headers experience the effects of creep under normal operating conditions. In addition to material degradation resulting from creep, high-temperature headers can also experience thermal and mechanical fatigue. In a boiler unit, header expansion may result in fatigue cracks at support attachments, moment restraints, superheater and reheater tubes, as well as header tubes to stub welds [2]. Failures have been reported in critical boiler header components subjected to thermal fatigue load applied in pressure vessels [3, 4]. The aforementioned literature clearly illustrate that failures may occur in tubes due to thermal fatigue. It is important to study the effect of thermal fatigue on tubes. Experiments on thermal fatigue of austenitic and duplex stainless steels subjected to cyclic thermal transients in the temperature range of 20-600°C have been performed. Experiments have been conducted by rapidly heating the specimens using high-frequency induction coils and then cooling by water spray [5]. Experimental setups have been developed to conduct thermal fatigue using furnace and quenching rig on a plain carbon steel plate. Complex nonlinear stress distributions and environmental effects occurring during thermal have also been studied [6, 7]. T11 heat exchanger used in ammonia plants subjected to thermal fatigue from 850°C to room temperature (25°C) have also been studied. The temperature 850°C was selected because these tubes were exposed to the process gas temperature of 960°C. Experiments have been conducted to confirm site failure results [8, 9]. Brown developed a hybrid method using finite element method to analyze the creep-fatigue life of boiler components

† This paper was recommended for publication in revised form by Associate Editor Dae-Eun Kim

*Corresponding author. Tel.: +91 431 250 3500, Fax.: +91 431 250 0133
E-mail address: psathiya@nitt.edu

Table 1. Chemical composition of ASTM A 213 GRADE T-92 material, filler wire and electrode [Vailant et al. [20]].

Materials	Elements (wt %)													
	C	Mn	P	S	Si	Cr	Mo	V	W	Nb	B	N	Al	Ni
ASTM A 213 GRADE T-92	0.09	0.50	0.020	0.010	0.50	9.20	0.40	0.20	1.90	0.06	0.004	0.050	0.040	0.40
GTAW filler wire	0.10	1.0	0.020	0.020	0.2	9	0.5	0.06	1.7	0.06	30-40 ppm	0.055	–	0.45
SMAW Electrode	0.09	1.1	0.013	0.007	0.30	9	0.5	0.25	1.7	0.07	30-40 ppm	0.05	–	0.45

Fig. 1. T-92 base tube before subjected to thermal fatigue.

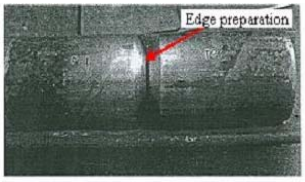

Fig. 2. Specimen after edge preparation.

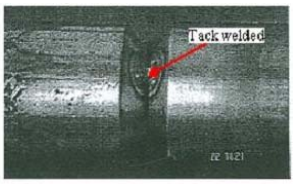

Fig.3. Specimen after tack welding.

[10]. The recent experience in the condition assessment of boiler header components used in fossil-fired power plants is discussed in [11, 12]. Tokiyoshi et al has carried out thermal fatigue test on perforated plate [13]. Kerezsi et al developed a test method for analyzing the initiation and growth of cracks in pressure vessels and piping equipment [14]. Thermal fatigue tests using laboratory procedure-induction coil and quenching rig for reproducing high temperature cracks found in coal fired boiler tubes have also been conducted [15, 16].

Previous studies have indicated that thermal fatigue is an important phenomenon for the development of crack in pressure vessel components, particularly in super-heater tubes. Studies have been carried out on thermal fatigue failure of boiler headers applying finite element model. However, simulating thermal fatigue behavior using the laboratory setup, while available, also have some constraints (dimensions and other conditions).

The objective of this paper is to study the effects of thermal fatigue on base and weld tubes, and determine the numbers of cycles necessary before failure occurs. In this work, a laboratory simulation reproducing thermal fatigue phenomenon was developed, and thermal fatigue tests were conducted on base and weld tubes, separately. The temperature and strain distributions along the specimen were computed theoretically using ANSYS software for the applied temperature condition. The tubes were subjected to thermal cycles from 800ºC to room temperature. The tests were carried out until open cracks were identified. The cause of the failure was thoroughly investigated in this paper.

Fig. 4. Weld specimen before subjected to thermal fatigue.

2. Experimental work

2.1 Specimen preparation

Two defect free ASTM A 213 grade T-92 tubes of 300 mm length, 48 mm outer diameter and 10 mm thickness were taken for this experimental study. One of the tubes was taken as base tube, as shown in Fig. 1.

Another tube was sectioned into two equal halves 150 mm in length, and the edges prepared for butt joining. The joint designs were selected as a single "V" joint. The edge preparation angle was 30º and the root face was 1mm as shown in Fig. 2. The joint fit up was tacked with manual metal arc welding (MMAW) as shown in Fig. 3.

The tack-welded tube was pre-heated to 220ºC using the tungsten inert gas (TIG) arc heating method. The root was gas tungsten arc (GTA) welded with CM91G filler wire at 85 amperes current and voltage of 17 V. The first and the second fill passes were welded with stick electrodes of 2.5 and 3.2 mm in diameter at 90-115 amperes, while the remaining three passes were welded using the SMAW process with thermanit MTS 616 electrodes of 125-135 amperes current. The necessary pre-heating was conducted at temperature of 220ºC for 109 s. After completion, the welding radiographic examination was conducted to ensure the quality of welds. The results were found to be within the acceptable range as per the ASME pressure vessel code requirements. The welded tube is shown in Fig. 4.

The chemical composition and mechanical properties of the T-92 tube, filler wire and electrode are given in Tables 1 and 2, respectively.

2.2. Experimental setup

An apparatus was built to conduct the thermal fatigue tests. The test setup employed in this study consisted of the following main physical components:

Table 2. Mechanical properties of ASTM A 213 GRADE T-92 material, filler wire and electrode [Vailant et al. [20]].

Materials	Ultimate tensile strength, UTS [MPa]	0.2%Yield strength, YS [MPa]	% of Elongation
ASTM A 213 GRADE T-92	620	440	20
GTAW filler wire	580	420	17
SMAW Electrode	760	420	20

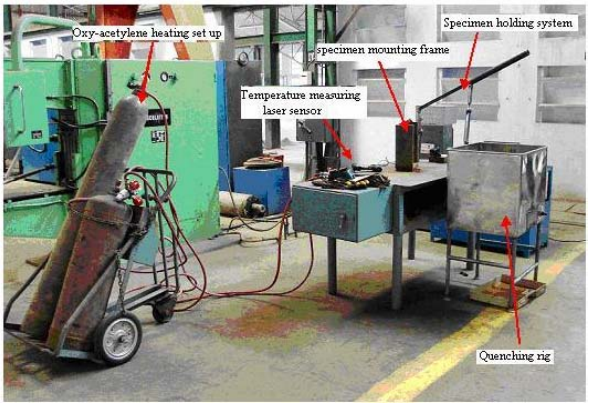

Fig. 5. Experimental setup.

1. The Oxy-acetylene heating set up
2. The specimen-mounting frame
3. The specimen-holding system
4. The quenching rig, and
5. The temperature-measuring laser sensor.

This set-up simulated the exact conditions of the heat exchanger tubes subjected to thermal fatigue. The specimen was locally heated up using the Oxy-acetylene torch from the outer surface of the tube. The peak temperature can be immediately attained through this process. The experimental set up is shown in Fig. 5.

2.3. Experimental procedure

The specimens were prepared as discussed above. Heat was applied from the outer surface of tube, which is the actual condition of a heat exchanger tube on pressure vessels exposed to thermal fatigue. The flame was applied to the heating zone manually, starting from one point of the heating zone and ending at the same point. The heat was uniformly distributed from the outer surface tube to the inner surface, as shown in Fig. 6. After one cycle, the temperature of specimen was measured using laser thermometer to check whether the temperature had reached the 800ºC. The time to attain 800ºC was 7 min. The flame was then switched off. The hot specimen was lifted with the help of a specimen-holding system and immersed into the quenching rig. When the temperature of the specimen had reached the room temperature, the specimen was removed from the quenching rig. The above process constituted one thermal fatigue cycle. A thermal cycle, which

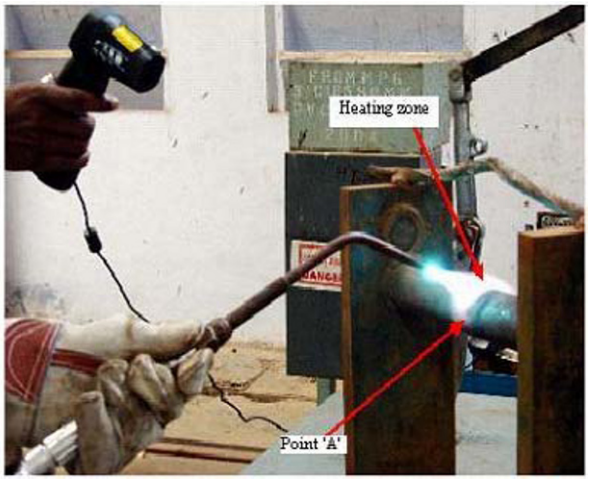

Fig. 6. Specimen mounting frame with heating.

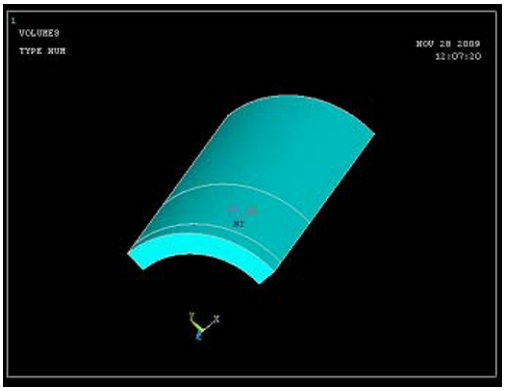

Fig. 7. Axis symmetric tube model using ANSYS.

included both the heating and cooling cycles, took 10 min to complete. The experiments were conducted until open cracks could be identified. The specimens were removed from the specimen-mounting frame using a power hacksaw; the specimens were subjected to Non destructive tests (NDT) tests and sectioned for metallographic study.

3. Finite element model

In this work, the tube is considered as an axis symmetric problem and the one-eighth portion of the tube was modeled for the analysis. The models were created using geometric primitives, which are fully developed lines, areas, and volume, as per the tube dimensions shown in Fig 7. The solid model was meshed to obtain the finite element model. Direct generation method is convenient for small and simple models, and provides complete control over the geometry and numbering of every node and every element. In this work, direct generation technique was adopted, and thermo-mechanical analysis was carried out [18, 19]. The tube was modeled using solid 70 and 45 elements for the thermal and structural analysis, respectively. The element sizes were made finer in the heated zone, since the temperature gradient was very high (stress

Table 3. Temperature dependent properties of T-92 material [Vailant et al. [20]].

Temperature (°C)	Coefficient of linear expansion ($\times 10^{-6}$/k)	Specific heat capacity (J/Kg K)	Thermal conductivity (w/mk)
20	11.18	420.384	36.556
100	11.452	432.04	36.26
200	11.792	453.81	35.89
300	12.132	483.58	35.52
400	12.472	521.35	35.15
500	12.812	567.12	34.78
600	13.152	620.89	34.41
700	13.492	682.66	34.04
800	13.832	752.43	33.67

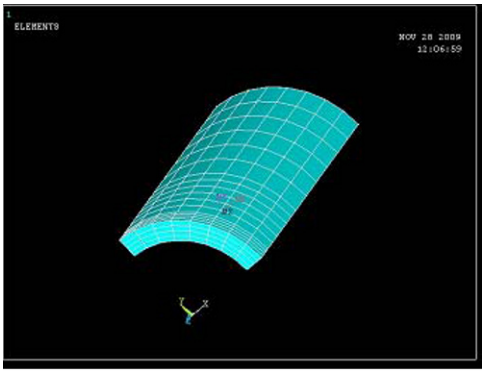

Fig. 8. Meshed model using ANSYS.

concentration). Coarser elements were used away from the heated zone. Four elements were used along the depth direction. Twenty-five divisions were made along the tube direction, while eight divisions were made for the transverse direction, as shown in Fig. 8. The material properties of T-92 tube are given in Table 3. The simulation work was carried out during ANSYS 10.0, and results were compared with the experimental results.

4. Results and discussion

The experiments were carried out until open cracks could be identified. Surface cracks were identified in the base and weld tubes after 90 and 60 cycles, respectively

4.1. Comparison of FEM results with experimental results.

Temperature and strain plots were used for finding the temperature and strain distribution on the heated tube. For the three-dimensional modeling, very fine mesh was chosen in order to achieve good results. The temperature distribution plot is shown in Fig. 9. A comparison of the experimental and analyzed results showed that the tube was normal before heating; after the thermal fatigue process, the tube's heated zone showed bulging in both conditions, as shown in Figs. 9 and 11, respectively. In this study, we arrested the linear expansion of

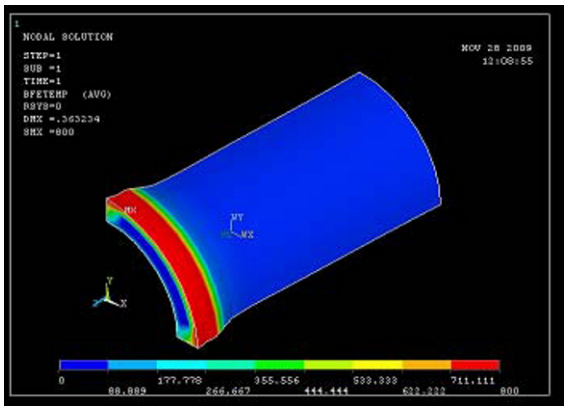

Fig. 9. Temperature contour plot on tube while heating at 800° C in the center.

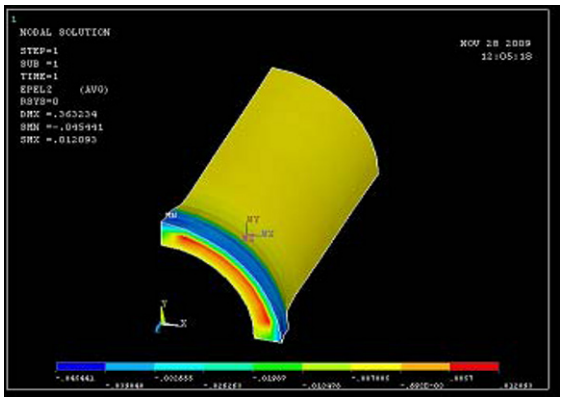

Fig. 10. Strain contour plot on tube after heating at 800° C in the center.

the tube by applying constrained condition to avoid the possibility of linear expansion during thermal fatigue. Thus, both tubes were shown to be bulged in the experimental and FEM analysis.

This indicates that the developed model showed similar characteristics with the experimental model. The strain distribution plot is shown in Fig. 10.

The simulated strain result showed a maximum value of 1.2×10^{-2} along the tube surface.

4.2. Visual inspection in failed tubes

The failed base and weld tubes were visually inspected and the developed crack in the tubes measured and presented below.

4.2.1 Visual inspection in failed base tube

The macrograph of the failed base tube is shown in Fig. 11. Fig. 11 illustrates that a number of surface cracks were observed in the base tube subjected to thermal fatigue after 90 cycles.

The cracks shown in Fig. 11 were measured and identified. A 5 mm long longitudinal crack and a transverse crack of 9 mm were visually identified in the failed base tube at the heated zone. The tube is bulged in the heating zone, which can

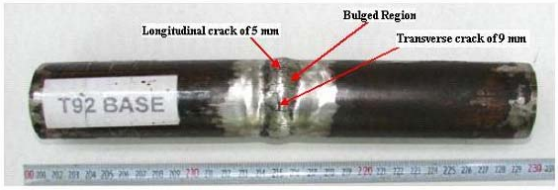

Fig. 11.Visual inspection of failed base specimen after subjected to thermal fatigue.

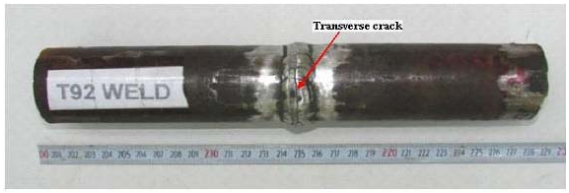

Fig. 12. Visual inspection of failed weld specimen after subjected to thermal fatigue.

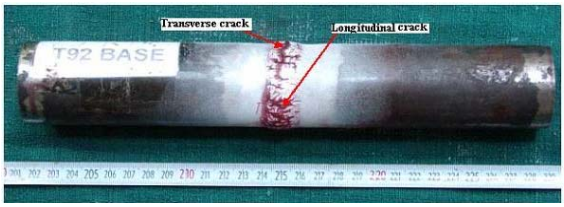

Fig. 13. Liquid penetrant examination of failed base specimen.

be clearly seen in Fig. 11. The failed tube was then subjected to liquid penetrant test to identify small surface cracks.

4.2.2 Visual inspection in failed weld tube

The macrograph of the failed weld tube is shown in Fig. 12, which shows that numerous surface cracks were observed in the base tube subjected to thermal fatigue after 60 cycles.

As shown in Fig. 12, a transverse crack 65 mm long was visually identified in the failed weld tube at the heated zone. The failed tube was then subjected to liquid penetrate test to identify small surface cracks.

4.3 Liquid penetrate test

To identify the small surface cracks on the failed tubes, the base and weld tubes were subjected to the liquid penetrate test.

4.3.1 Liquid penetrate test on the failed base tube

The macrograph of the failed base specimen subjected to liquid penetrate test is shown in Fig. 13, which clearly shows that a number of longitudinal cracks in the heated zone. Several small transverse cracks could also be identified from the longitudinal crack.

4.3.2 Liquid penetrant test on failed weld tube

Fig. 14 shows the macrograph of the failed weld specimen subjected to liquid penetrate test. The Fig. clearly shows that

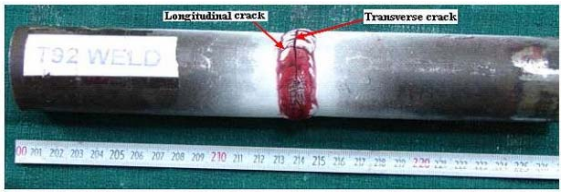

Fig. 14. Liquid penetrate examination of failed weld specimen.

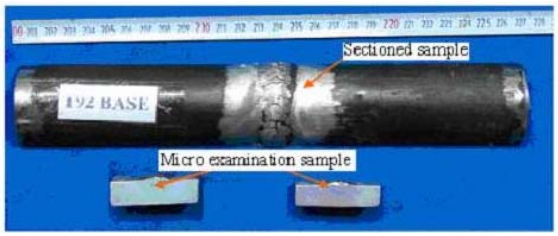

(a)

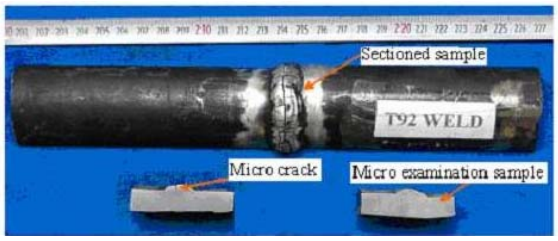

(b)

Fig. 15. Sectioned view of the failed base and weld tubes.

numerous transverse cracks had developed in the heated zone, which traveled throughout the circumference of the weld. Small longitudinal cracks were also seen from the transverse crack, which had been invisible in the visual examination.

The failed tubes were then sectioned and subjected to metallographic study.

4.4 Specimen preparation for metallographic study

The sectioned views of the failed base and weld tubes are shown in Fig. 15(a and b). The failed tubes were sectioned in two halves in the longitudinal direction, and one of the halves was further divided into two sections. The projected portion from the two sides of the heating zone in the tube was also removed so that only the heated zone was taken for metallographic study. Specimens for the metallographic examinations were prepared by polishing successively in 220, 320, 400, 600, 800 emery grits, followed by a disc polishing cloth. The specimens were etched with 4% Nital solution. The specimens were then subjected to microscopic and scanning electron microscopy (SEM).

4.5 Macro study

Before being subjected to micro-analysis, the polished samples were subjected to macro study. Macro photographs of the outer surface of the failed tubes were taken to obtain a closer view of the cracks in the surface, while the photographs of the

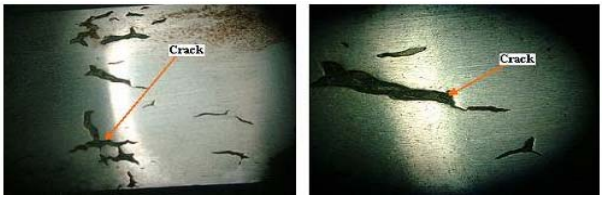

(a) (b)

Fig. 16. Magnified view of the surface crack obtained in the failed base tube.

(a) (b)

Fig. 17. Magnified view of the surface crack obtained in the failed weld tube.

microstructure in the cross-section of the failed tube on the thickness side were taken to study the depth of penetration of the crack.

4.5.1 Macro study on the failed base tube

Fig. 16(a) shows a magnified view of the surface crack observed in the failed base tube subjected to thermal fatigue. It clearly illustrates that numerous longitudinal cracks developed in the heated zone, while numerous small transverse cracks also developed from the longitudinal crack. Fig. 16(b) shows a magnified view of the single longitudinal crack obtained in the failed base tube.

4.5.2 Macro study on the failed weld tube

Fig. 17(a) shows the magnified view of the surface crack observed in the failed weld tube subjected to thermal fatigue. It clearly shows that numerous transverse cracks developed in the heated zone, and that small longitudinal cracks also developed in the transverse crack. Fig. 17(b) shows the magnified view of the surface crack observed in the failed weld tube.

4.6 Optical microscopy

The samples were prepared according to ASME standards. The polished and etched samples were examined under optical microscopy and SEM. The microstructures were taken on different locations of the tubes in the defect and defect-free surfaces.

4.6.1 Study on the failed base tube

The metallographic samples prepared from the failed base tube were studied by optical microscope in both the defect and defect-free regions.

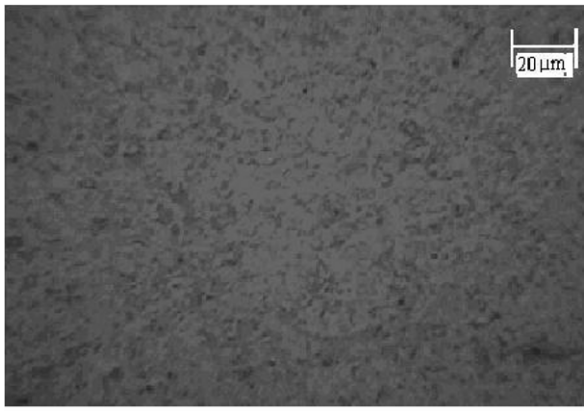

Fig. 18. Microstructure of base in defect-free region.

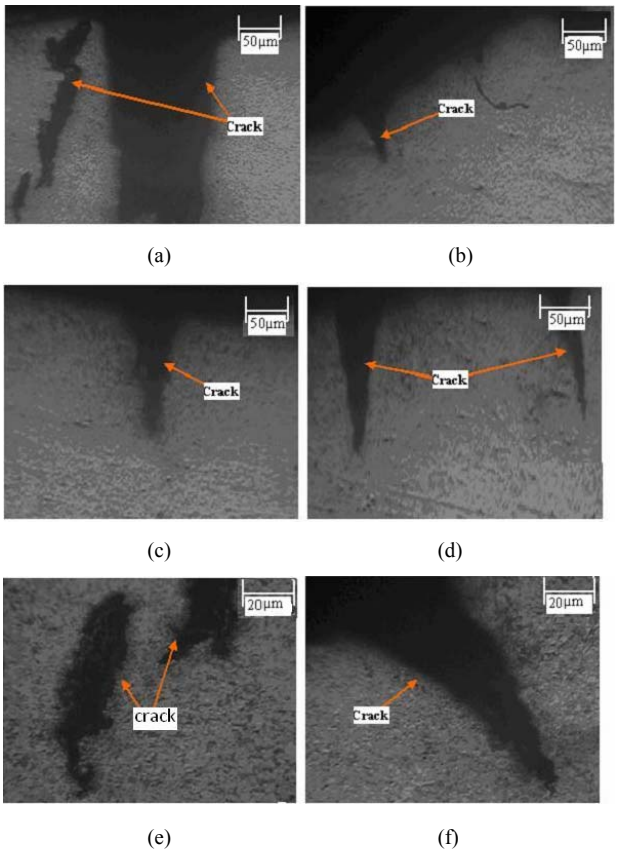

(a) (b)

(c) (d)

(e) (f)

Fig. 19. Cracks identified in the failed base tube.

4.6.1.1 Study on the defect free surfaces on the failed base tube

The microstructures of defect-free surfaces of the failed base tube are shown in Fig. 18.

Fig. 18 shows the optical microstructure of T-92 failed base tube taken in the defect-free surface. The microstructure of T-92 failed base tube showed a larger grain size. The dark-colored grains seen in the microstructure are tempered martensite. The tempered martensite provides the alloy high-creep strength by precipitation hardening. Formed carbides and

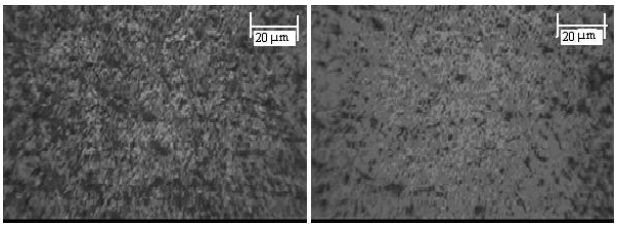

(a) (b)

Fig. 20. Microstructure of base and weld region in defect free areas.

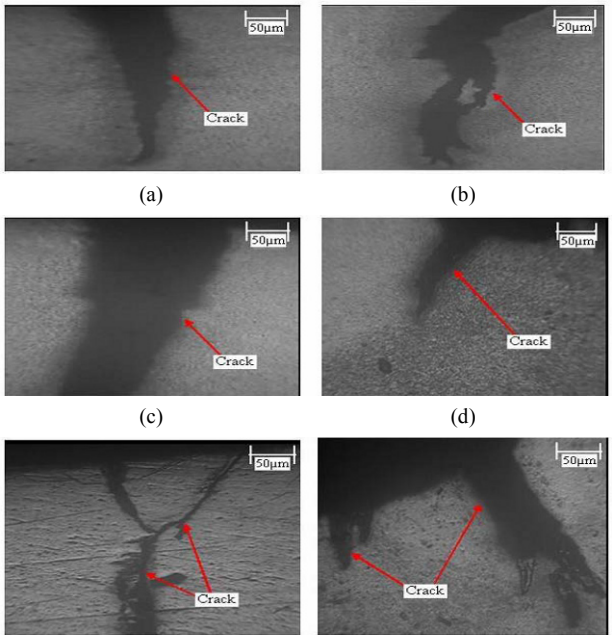

(a) (b)

(c) (d)

(e) (f)

Fig. 21. Cracks identified in the failed weld tube.

carbo-nitrides were found on the grain boundaries. The higher degree of hardness was due to the tempered martensite and carbides.

4.6.1.2 Study of the defect surfaces on the failed base tube

The defect surfaces in the T-92 base tube were identified through optical microscope, as presented in Figs. 19(a-f). The figures clearly illustrate a large number of cracks in the failed base tube. The cracks developed from the heating surface (outer surface) of the tube and traveled towards the inner surface. Oxide-filled blunt-tipped parallel cracks were also observed, which appear to have similar characteristics as the thermal fatigue failure. Decarburization of the grains nearer to the crack edges was also observed. Cracks observed in the failed base tube closely resembled the cracks observed in the failed tubes [8].

4.6.2 Study on the failed weld tube

The metallographic samples prepared from the failed weld tube were studied thoroughly using the optical microscope on both the defect and defect free regions.

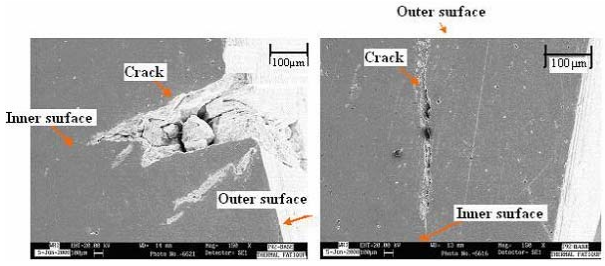

(a) (b)

Fig. 22. Crack propagation in the failed base tube.

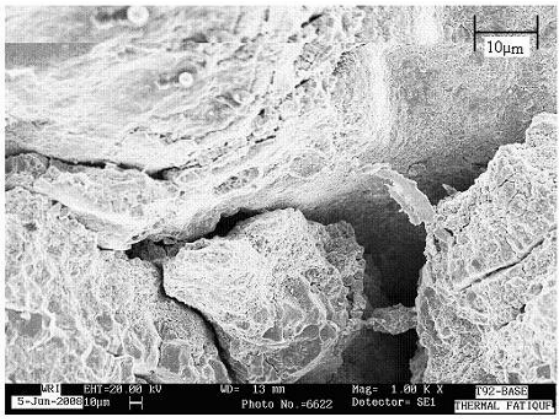

Fig. 23. Cracking along the grain boundaries.

4.6.2.1 Study on the defect free surfaces on the weld tube

The microstructures of defect free surfaces of the failed weld tube are shown in Fig. 20(a and b).

The microstructures of the base and weld surfaces taken from the defect-free portion of the welded tube are shown in Fig. 20(a and b). The grains were coarser than the base metal because the cooling rate of the heat affected zone [HAZ] in welding was much higher than that during the manufacture of the metal. The high cooling rate resulted in irregularly shaped grains and decreased strength since the amount of carbides formed was less due to low rate of precipitation. The microstructure showed irregular grains and the formation of martensite due to high cooling rate. Since the grains were coarser, they have a higher tendency towards cracking.

4.6.2.2 Study on the defect surfaces on the weld tube

The defect surfaces in the T-92 weld tube were identified through optical microscope, as presented in Fig. 21. The figures clearly illustrate a large number of cracks present in the failed weld tube. The cracks developed from the heating surface (outer surface) of the tube and propagated towards the inner surface. Oxide-filled blunt-tipped parallel cracks were also observed, which appear to have similar characteristics as with that of thermal fatigue failure. Decarburization of the grains nearer to the crack edges was also observed. The cracks observed in the weld tube closely resembled the cracks ob-

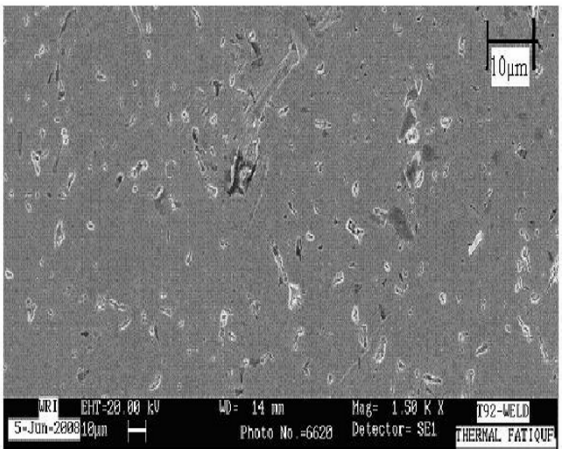

Fig. 24. Unaffected weld tube structure.

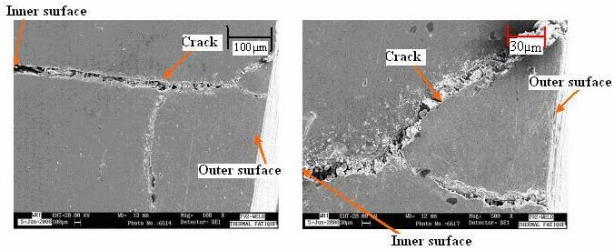

(a) (b)

Fig. 25. Crack propagation in the failed welded tube.

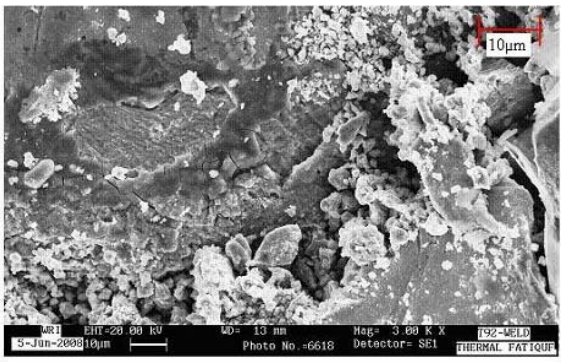

Fig. 26. Cracking along the grain boundaries.

served in the failed tubes, as reported in the ASM handbook [16].

4.7 SEM study

The cracks observed in the optical microscope were subjected to the SEM study to analyze the failures in detail. SEM analyses were carried out on the defect surfaces of the base and weld tubes.

4.7.1 Defect surface on failed base tube

The cracks observed in the SEM examination of the failed base tube are shown in Fig. 22(a and b). Figs. 22(a and b) show that the cracks developed from the outer surface of the

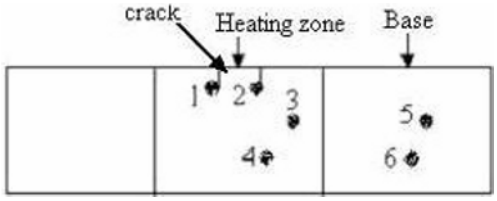

Fig. 27. Hardness locations taken in the failed base tube.

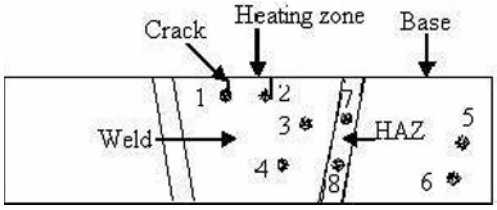

Fig. 28. Hardness locations taken in the failed weld tube.

tube and propagated towards the inner surface. Similarly, the cracks traveled in the circumference of tube-heated region. When they were compared to the cracks obtained in the failed weld tube, the width and depth of the cracks were less. This is clearly shown in Figs. 22(a and b). Crack formation was observed inside the cracked surface at higher magnification. Upon further magnification of the cracked surface, grain boundary cracks were clearly seen, as shown in Fig. 22. Figs. 22(a and b) clearly identify that the position of the crack width was initially high, which then moved towards the inner surface. The crack growth rate increased due to the temperature difference and rate of cooling, which are the reasons for the development of the cracks.

4.7.2 Defect surface on failed weld tube

Fig. 24 shows the microstructure taken in the unaffected region of the failed weld tube. The defects present in the failed weld tube are shown in Figs. 25(a and b). Figs. 25(a and b) clearly show that the cracks developed from the outer surface of the tube, which then traveled towards the inner surface. Similarly, it traveled in the circumference of tube's heated region. When compared to the base cracks, the cracks obtained in the weld were larger. Crack formation was observed inside the cracked surface at higher magnification. Upon further magnification, grain boundary cracks were clearly seen, as shown in Fig. 25. Figures 26 (a and b) show the position of the crack width was initially high; the crack growth rate increased as it moved towards the inner surface due to the temperature difference and rate of cooling.

Upon evaluating the micro study and SEM results, it is apparent that the cracks developed from the heating surface (outer surface) of the tube and traveled towards the inner surface, which eventually caused the failure of the tube. The cracks that occurred in the tube were due to the long exposure to service temperature. Grain boundary cracks were also observed inside the crack at higher magnification. The cracks obtained in the tube specimen were the typical thermal fatigue crack, which resembled the failures reported in the tubes sub-

Table 4. Hardness taken in the base tube.

Position	Base	Heating zone	Near the crack
Before being subjected to thermal fatigue	252,260	____	____
After failure occurs	280,272	473,478	503,493

Table 5. Hardness taken in the weld tube.

Position	Base	Weld	Haz	Heating zone	Near the crack
Before being subjected to thermal fatigue	252,260	266,258	240,236	____	____
After failure occurs	270,284	405,429	292,297	405,429	483,486

Table 6. Comparison of number of cycles to failure for base and welded tubes.

Materials	Base tube	Welded tube	Difference
ASTM A 213 Grade T-23	120	80	40
ASTM A 213 Grade T-91	85	53	32
ASTM A 213 Grade T-92	90	60	30

jected to thermal fatigue [16].

4.8 Hardness

Hardness measurements were taken on the base and welded tube materials before being subjected to thermal fatigue. After failure occurred, hardness was determined according to the Vickers hardness test. The hardness location taken in the base and welded tube specimens are shown in Figs. 27 and 28. The load applied was 10 kg. The hardness values taken from the base and welded tube materials are tabulated in Tables 4 and 5.

Table 3 and 4 illustrate that the hardness value was much higher nearer the crack zone. Due to the higher hardness, the cracks initiated due to the thermal fatigue were propagated towards the circumferential areas and through the thickness of the tube. The hardness values of the weld nearer to the crack zone were closer to the heating zone. Due to repeated heating and cooling, the grains became finer, and the hardness values were increased when compared to the base material.

4.9 Comparison of number of cycles to failure occurs in T-23, T-91, and T-92 base and welded tubes

Thermal fatigue tests were similarly carried out on the T-23, T-91, and T-92 base and welded tubes until failure occurred. Table 6 provides the number of cycles until failure in base and welded tubes.

Table 6 shows that base tubes can withstand more cycles when compared to weld tubes when subjected to thermal fatigue. An average difference of 35 cycles was obtained for all grade tubes. The reason for the failure of the welded tube was due to the lesser number of cycles, which shows that weld is the weakest area in a joint for the development of the crack.

5. Conclusion

The following conclusions can be drawn from this research work.

The effects of thermal fatigue on ASTM A 213 GRADE T-92 base and weld tubes have been studied effectively.

While the thermal cycling surface cracks can be identified in the base and weld tubes after 90 and 60 cycles, respectively, the base tube can withstand 30 cycles more when compared to the welded tubes subjected to thermal fatigue.

While thermal cycling T-23 tubes cracks can be identified after 120 cycles, T-23 is more suitable for high-temperature applications when compared to T91 and T92 tubes.

FEM has been simulated as per the designed matrix. The temperature and strain contours for the heated tubes have been obtained to study the effect of thermal fatigue. A comparison between the simulated temperature contour and the failed thermal fatigue tubes yield a bulging of the tube in the heated zone. The simulated strain result shows a maximum value of 1.2×10^{-2} along the tube surface.

Through visual examination, a 5 mm long longitudinal crack can be visually identified in the failed base tube at the heated zone. The tube is bulged in the heating zone, which can be clearly seen. A transverse crack 65 mm long can be visually identified in the failed weld tube at the heated zone. This illustrates that longitudinal cracks develop in the base tube during thermal fatigue, and that transverse cracks occur in the welded tube.

Liquid penetrant test showed that apart from longitudinal cracks, small transverse cracks also occur in the failed base tube. Similarly, in the welded tube, apart from the transverse crack, small longitudinal cracks also occur.

Cracks can be observed from the macro and the micro examinations. These defects are seen both in the failed base and in the welded tube specimens. The cracks develop from the outer surface of the tube and travel towards the inner surface of the tube.

In the SEM examination of the cracks, grain boundary cracks can be observed inside the crack at higher magnification.

The hardness test showed that at the point nearer to crack the hardness value is much higher. Due to the higher hardness, cracks that develop through the thermal fatigue process are propagated toward the circumferential areas and through the thickness of the tube. The hardness value of the weld nearer to the crack zone is closer to the heating zone. Due to repeated heating and cooling, the grains become finer and the hardness values are increased when compared to the base material.

The development of these cracks is due to the temperature variation from high temperature to room temperature during the plant operation during the start up and shut down.

References

[1] M. Hayashi, Thermal fatigue behavior of thin-walled cylin-

drical carbon steel specimens in simulated BWR environment, International Journal of Nuclear Engineering and Design, 184 (1998) 123-133.

[2] T. Yoshimoto, S. Ishihara, T. Goshima, A. J.McEvily and T. Ishizaki, An improved method for the determination of the maximum thermal stress induced during a quench test, Scripta Materialia, 41 (5) (1999) 553-559.

[3] A. Tulyakov, Thermal fatigue in heat power engineering, Mashinostroyeniye, 197 (1978).

[4] A. B. Vainman, R. K. Melekhov and O. D. Smiyan, Hydrogen induced embitterment of high- pressure boiler elements. Kyiv, Naukova Dumka, 272 (1990).

[5] Virkkunen Iikka, Thermal fatigue of austenitic and duplex stainless steels. Acta Polytechnica Scandinavica, Published by the Finnish Academies of Technology Mechanical Engineering Series No. 154 Espoo (2001) 115.

[6] B. B. Kerezsi, J. W. H. Price and R. N. Ibrahim, Using S–N curves to analyse cracking due to repeated thermal shock, Journal of Materials Processing Technology, 145 (2004) 118-125.

[7] H. C. Young and Y. C. Sun, Socket weld integrity in nuclear piping under fatigue loading condition, Nuclear Engineering and Design, 237 (2007) 213-218.

[8] A. Usman and A. Nusair Khan, Failure analysis of heat exchanger tubes, Engineering Failure Analysis, 15 (2007) 118-128.

[9] A.Shiblia and F. Starr, Some aspects of plant and research experience in the use of new high strength martensitic steel T91, International Journal of Pressure Vessels and Piping, 84 (2007) 114-122.

[10] T. B. Brown, Assessing the effect of thermal transients on the life of boiler plant, Babcock Energy Limited, Scotland (1998).

[11] J. P King and D. B. Riley, Inc. Worcester, Massachusetts, Recent experience in condition assessments of boiler header components and supports, Presented at the 1996 ASME Pressure Vessels and Piping Conference , (1996) July 21-26.

[12] I. R. Paterson and J. D. Wilson, Use of damage monitoring systems for component life optimization in power plant, International Journal of Pressure Vessels and Piping,79 (2002) 541-547.

[13] T. Tokiyoshi, F. Kawashima, T. Isari and H.Kino, Crack propagation life prediction of a perforated plate under thermal, International Journal of Pressure Vessels and Piping, 78 (2001) 837-845.

[14] B. B. Kerezsi, A. G. Kotousov and J. W. H. Price, Experimental apparatus for thermal shock fatigue investigations, International Journal of Pressure Vessels and Piping, 77 (2000) 425-434.

[15] B. J. Smith, C. I. Erskine, R. J. Hartranft and A. R. Marder, High-Temperature Corrosion-Fatigue (Circumferential) Cracking life Evaluation Procedure for low Alloy Cr-Mo) Boiler Tube Steels, Lehigh University, Bethlehem, PA 18025 (1999).

[16] E. E.Underwood and K. S Banerji, Fractal analysis of fracture surfaces, ASM Hand Book, formerly Ninth edition, Metals Handbook, volume-12 (2000).

[17] P. E Daniel J Benac and V. P. Swaminathan, Elevated-Temperature life assessment for turbine components piping and tubing failure analysis and prevention, ASM Handbook, volume 11.

[18] V. J. Papazoglou and K. Masubuchi, Numerical analysis of thermal stresses during welding including phase transformation effects, Journal of Pressure Vessel Technology, 104 (3) (1982) 198-203.

[19] J. N. Reddy, On penalty function methods in the finite element analysis of flow problems, International Journal For Numerical Methods, 2 (2) (1982) 151-171.

[20] J. C Vailant, B. Vanderberghe and C. Zakine, The T23/ P23, T22/ P22, T91/ P91, T92/ P92, Book, Vallourec & Mannesmann tubes.

P. Sathiya 2006 Doctoral Thesis on Friction welding of similar stainless steels and Evaluation of processed joints, Bharathidasan University, Tiruchirappalli, Tamilnadu, India. 1996 Master degree on Welding Engineering, Regional Engineering College, Bharathidasan University, Tiruchirappalli, Tamilnadu, India. 1994 Under graduate Degree on Mechanical Engineering, Government college of Engineering, Salem, University of Madras, Tamilnadu, India. Assistant Professor, Department of Production Engineering, National Institute of Technology, Tiruchirappalli, Tamilnadu, India. I am working in the area of Welding Technology, Solid state Joining, Materials Behaviour Subjected to Welding, Similar and Dissimilar Materials Welding, Failure Analysis of Weldments, Modeling, Simulation of Welding processes and Welding parameter optimization. I received young technology award 2009, from Indian Welding Society, India and also received young scientist award from Department of Science and Technology, New Delhi, India. Published thirty papers in international and national reputed journals.